Int. J. Electrochem. Sci., 13 **(2018)** 9317 – 9332, doi: 10.20964/2018.10.37

International Journal of ELECTROCHEMICAL SCIENCE
www.electrochemsci.org

Influence of Solvents and Irradiation time on Structural and Optical Properties of Cubic PbS Nanoparticles

M N Maharaz[1,3], M K Halimah[1,], S Paiman[1], N. M Saiden[1], I M Alibe[2,4]*

[1] Department of Physics, Faculty of Science, Universiti Putra Malaysia, 43400 UPM Serdang, Selangor, Malaysia
[2] Material Synthesis and Characterization Laboratory (MSCL), Institute of Advanced Technology (ITMA), Universiti Putra Malaysia, 43400 UPM Serdang, Selangor, Malaysia
[3] Departments of Physics, Federal University Dutse, Jigawa State, Nigeria
[4] National Research Institute for Chemical Technology Zaria, Kaduna State Nigeria
[*]E–mail: hmk6360@gmail.com

Received: 2 March 2018 / *Accepted:* 3 July 2018 / *Published:* 1 September 2018

In the present paper, different particle sizes of lead sulfide (PbS) nanoparticles with a cubic structure were successfully prepared using a microwave irradiation method from lead acetate [$(CH_3COO)_2Pb.3H_2O$] and thioacetamide (CH_3CSNH_2) as the starting materials. Ethylene glycol ($C_2H_6O_2$), distilled water (H_2O), ethylene alcohol (C_2H_5OH) and isopropanol (C_3H_8O) were used as solvents and a 650W oven operating at 20% of the nominal power in the period of 10 min was employed. The effect of the microwave irradiation time was investigated by varying the irradiation time from 10 to 50 minutes respectively. The resulting nanoparticles in different sizes were characterized using X–ray diffraction, Transmission electron microscopy (TEM) and UV–Vis absorption spectroscopy. The crystallite sizes were calculated from the broadening of the XRD peak using Scherrer's equation. The results showed that the increased intensity of the XRD peak and the dipole moment of the solvents being decreased corresponded with the reduction in particle sizes. The TEM results indicated that the samples consisted of separated, well–defined spherical particles and showed a small distribution size. As can be seen from the UV–vis spectrum, the band gap energy of each sample had increased and showed a characteristic blue shift due to the quantum confinement in their optical absorption. The mechanism that influenced the solvents and irradiation time for the formation of the PbS nanoparticles were discussed.
.

Keywords: Lead sulfide; Solvents; Nanoparticles; Microwave Irradiation; Band gap energy

1. INTRODUCTION

Nanoparticles with different particles sizes and morphology may open new opportunities for exploring their physical and chemical properties, and immense efforts have been devoted to controlling the nanoparticles of materials in terms of size, shape, and dimension. Recently, the focus of research has been on semiconductor nanoparticles due to their outstanding electronic and optical properties and extensive application potential in various devices including light–emitting diodes [1], single electron transistors [2], field–effect thin–film transistors [3] and electrochemical nanosensors [4]. Different forms of nanoparticles with different sizes and compositions of semiconductor have been used for constructing electrochemical sensors and biosensors, and these nanoparticles play significant roles in different electrochemical sensing systems [5, 6]. The significant functions provided by nanoparticles such as immobilization of biomolecules, the catalysis of electrochemical reactions, the enhancement of electron transfer between electrode surfaces and proteins, labeling of biomolecules and even acting as reactant [7].

Fundamentally, the electronic and optical properties of semiconductor nanoparticles are tunable by varying their shapes and sizes [8]. One of the desired goals in nanoparticles research is to realize precise control of the particle size and morphology of the materials. Semiconductor nanoparticles possess various unique properties which vary from those of corresponding bulk materials due to the three–dimensional confinement of electrons and holes in a small volume or the fact that the number of atoms on the surface is more comparable to that inside the particles [9, 10]. The surface of nanoparticles is more relevant than the bulk as regards to its properties, as nanoparticles have a larger surface–to–volume ratios. Weaker forces bind surface atoms because of the missing neighbours, which lead to high surface reactivity. The surface is the stage on which chemical reaction, sublimation, adsorption, and disruption occur. Due to that, there has been considerable interest in developing semiconductor nanoparticles [11-13]. Nanoparticles can be prepared in the form of dispersed colloids or trapped and stabilized within micelles [14], polymers [15], zeolites [16], or glass [17]. In some cases, nanoparticles prepared by these techniques have poorly surfaced exterior and a relatively broad size distribution. Microwave irradiation is a heating process that is extensively quick, uncomplicated and efficient in energy; it is relatively advanced and is generally used in various research fields [18].

It is generally known that dielectric heating is generated due to the interaction of dielectric materials, liquid or solid with microwave. Electric dipoles present in the dielectric substances respond to the applied electric field. In polar solvents, this permanent reorientation causes friction between the entire molecules, which finally generate heat. The claimed effects of microwave irradiation consist of thermal and non–thermal effects [19]. Recently, organic solvents including formaldehyde [20],benzene, tetrahydrofuran, triethylene tetraamine [21], ethylenediamine [22, 23], have been introduced into the preparation of metal chalcogenides. As a result of the different properties of the organic solvents including viscosity, polarity, and softness, various synthetic environments could be observed, which would affect the solubility and carrier behaviour of the precursors. As a result, they influence the surface morphology and size of the final products [24]. Presently, only a few pieces of

literature have been reported on the microwave irradiation synthesis of PbS nanocrystals in various solvents. Qiao et al. (2015) reported the preparation of nanocrystalline PbS in ethanol by employing gamma–radiation method [25].

The use of microwave irradiation in numerous fields of research has experienced very rapid growth because of particular reaction effects, including rapid volumetric heating and the indirect dramatic increase in the reaction rates. PbS semiconductors have been used in various applications such as light–emitting diodes, infrared detectors, optic fibers, infrared lasers, window coatings, and solar energy panels [26]. This large panel of applications is due to its interesting physical properties such as Bohr exciton radius (18nm), small effective electron and hole masses, a large optical dielectric constant and an infrared direct band gap in the bulk state (0.41 eV at 298 K), which corresponds to an absorption onset at 3024 nm [27]. In the near–infrared, PbS has a good photoconductive property. In this work, the effect of solvents and time of irradiation in the formation of PbS nanoparticles sizes will be investigated. This attempt can be studied by seeing the optical and structural properties of the synthesized materials. In addition to that, the final results will also be related to the potential applications of electrochemical and photoelectrochemical studies.

2. EXPERIMENTAL

2.1. Materials and instruments

Lead (II) acetate trihydrates [$(CH_3COO)_2Pb.3H_2O$] (MW 379.33g/Mol,) and thioacetamide (CH_3CSNH_2) (MW: 75.13g/Mol, 99.0%) were used as lead and sulfur sources respectively. Distilled water (H_2O), Ethylene glycol ($C_2H_6O_2$), Ethylene alcohol (C_2H_5OH) and Isopropanol (C_3H_8O) were used as solvents. Lead acetate was purchased from R & M Chemical, thioacetamide from Sigma–Aldrich, and solvents from ALFA Chemical Co. All chemicals are analytical grade products and used without further purification.

2.2. Synthesis

In a typical synthesis, 0.01g of lead acetate was added into a glass beaker of 500 ml containing 40 ml of aqueous sulfur solution (ethylene glycol (EG) and thioacetamide) and magnetically stirred at 500 rpm for 30 min so as for obtaining a homogeneous solution. The beakers were placed in a high power microwave oven (650 W, 2.45 GHz) operated using a pulse regime with 20% power. The reactions were carried out at 10 min irradiation time. The precipitates were centrifuged (3500 rpm, 5 min) and washed with deionized water repeatedly. The dark brown products were obtained and dried in a vacuum oven at 60 ℃. The same procedure was repeated using distilled water (H_2O), ethylene alcohol (EtOH) and isopropanol (ISO), respectively. Thus, the samples are named based on solvents used; PbS–EG, PbS–H_2O, PbS–EtOH, and PbS–ISO, respectively. For the investigation of the effect of

irradiation time on nanoparticles sizes, the same procedure was applied with varying the irradiation time from 10,15,45 and 50 min with ethylene alcohol as a solvent, this solvent is proposed due to its intermediate dipole moment among the solvents.

The final products were characterized by X–ray diffraction (XRD) at a scanning rate of 5^{o}/min in the 2θ range 20–70° using a Philips X–ray diffractometer (7602 EA Almelo) with Cu Kα radiation (λ = 0.1542 nm). The particle size and size distribution were determined from the transmission electron microscopy (TEM) micrographs (HITACHI H–7100 TEM). The TEM characterization was carried out at 100 keV. The optical properties of PbS nanoparticles were characterized using UV–visible absorption spectroscopy (UV–1650PC SHIMADZU). Figure 1 represents the schematic of the formation of PbS nanoparticles.

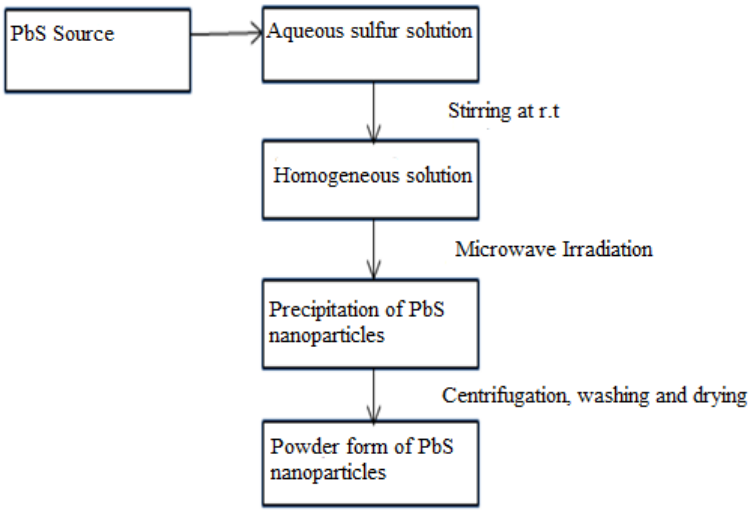

Figure 1. A schematic of the formation of PbS nanoparticles

3. RESULTS AND DISCUSSION

3.1. The Formation process of PbS nanoparticles

During the process, microwave irradiations provided the energy for the decomposition by accelerating the nucleation of the nanoparticles and depressing the growth of the new form of PbS nuclei due to the collisions that the molecules created and the intense friction. The reaction process for forming the PbS nanoparticles in ethylene glycol (EG) and the other solvents depended on the degree of temperature which decomposes thioacetamide and releases S^{2-} ions homogeneously. This promotes the rate of nucleation and growth of PbS nanoparticles, according to the following chemical reactions:

$$CH_3CSNH_2 \rightarrow CH_3CN + H_2S \quad (1)$$

$$H_2S + Pb(A_c)_2 \rightarrow PbS(nanoparticles) + 2HA_c \quad (2)$$

Equation (1) represents that the decomposition of thioacetamide (CH_3CSNH_2) using microwave heating. CH_3CN and H_2S would be formed. Further, H_2S reacts with $Pb(A_c)_2$ to create PbS nanoparticle. Equation (2) shows the result.

3.2. Influence of Solvents on particle sizes

Fig 2 shows the X–ray diffraction pattern for the four samples PbS–EG, PbS–H_2O, PbS–EtOH, and PbS–ISO, respectively. The diffraction peaks indicate the nanocrystalline nature with peaks at the angles (2θ) of 25.978, 30.085, 43.066, 50.985, 70.949, 53.427, 78.948, 68.894 and 62.541correspond to the reflection from: (111), (200), (220), (311), (222), (400), (331), (420), and (422) crystal planes which can be filed to the structure of pure cubic lead sulfide (ICDD PDF 96–900–8695) with 5.93 A° as the lattice parameter, respectively.

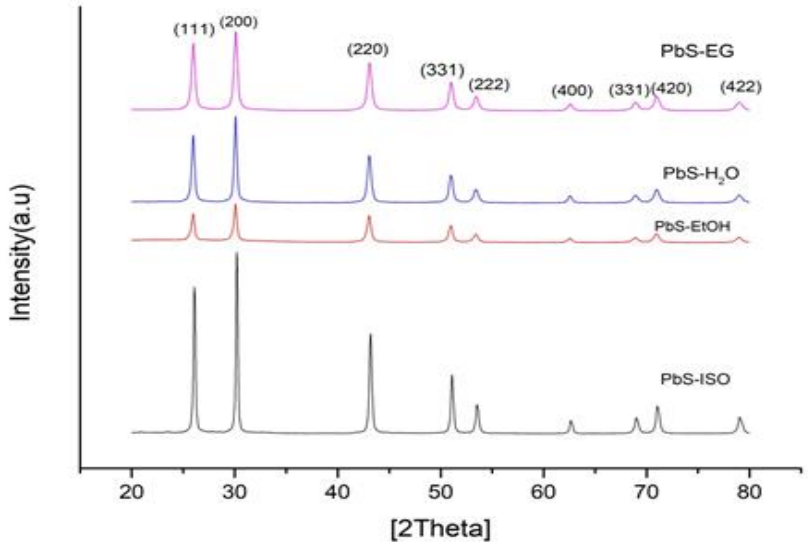

Figure 2. X–ray diffraction patterns of PbS nanoparticles prepared in various solvents by microwave irradiation method: Ethylene glycol (EG), Distilled water (H_2O), Ethylene alcohol (EtOH), and Isopropanol (ISO)**.**

In these samples, the (200) plane is the most intense peak, which indicates the preferential growth of the crystals in this particular direction. The average crystal sizes (D) were calculated based on the width of the peak due to the (200) planes by using the Scherrer's formula [28]:

$$D = \frac{0.94\lambda}{\beta Cos\theta} \qquad (3)$$

Where λ is the wavelength of X–ray used, β is the full width at half maximum (FWHM) and θ is the Bragg's angle of reflection. The average crystallites sizes (Table 1) calculated from Equation (3) imply that the crystallites size of the nanoparticles decreases with the increasing dipole moment of the solvents which corresponds with the increases of XRD peaks broadening (FWHM).

Table 1. X–ray diffraction results of PbS nanoparticles

Samples	Solvents	FWHM of $(200)(2\theta)$	Intensity of $(200)(2\theta)$	Crystallite sizes (nm)
PbS–EG	$C_2H_6O_2$	0.4560	11141.5	34.8
PbS–H_2O	H_2O	0.3910	12145.6	39.2
PbS–EtOH	C_2H_5OH	0.3346	5083.96	46.5
PbS–ISO	C_2H_8O	0.2351	26032.4	56.7

Fig 3 shows the TEM images of the particle sizes, particle distribution and the homogeneity of the nanoparticles. The results also show that the images are in spherical form and distributed homogeneously. Table 2 provides the TEM result, respectively.

Based on the UV–vis absorption study, the optical band gap of the nanoparticles are estimated to correspond to the transition from the valence bands to the conduction bands using the following equation:

$$\alpha(\nu) = A\left(h\nu/2 - E_g\right)^{m/2} \qquad (4)$$

Where α is the absorption coefficient, A is a constant related to the material properties, $h\upsilon$ represents the energy of a photon, E_g is the optical band gap and m equals 1 for a direct transition. Figure 4 shows the UV–vis absorbance spectrum of the samples. The two peaks are observed, the lower peak is observed at around 250 nm, and the higher is observed at around 550 nm. Both the peaks can be assigned to the exciton transitions. The energy intercept of a plot of $(\alpha h\upsilon)^2$ versus $h\upsilon$ yields the band gap energy, E_g for a direct transition (Fig. 5) [29].

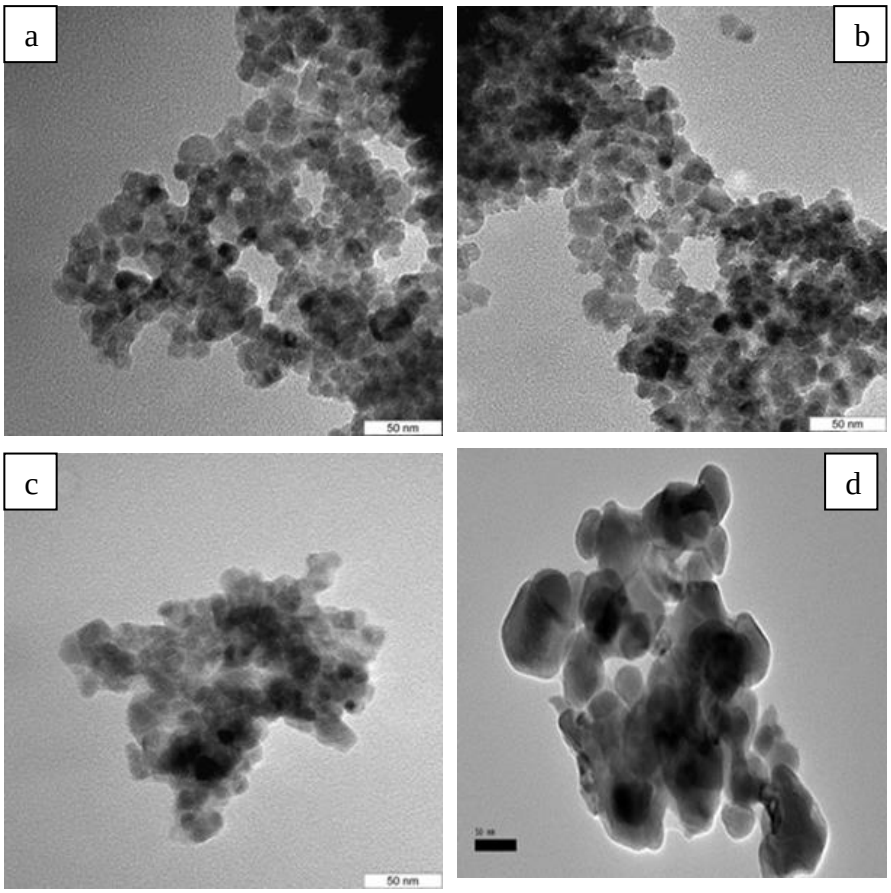

Figure 3. The TEM Images of as–prepared PbS nanoparticles synthesized under microwave irradiation in various solvents: (a) Ethylene glycol (EG), (b) Distilled water (H_2O) (c) Ethylene alcohol (EtOH), and (e) Isopropanol (ISO).

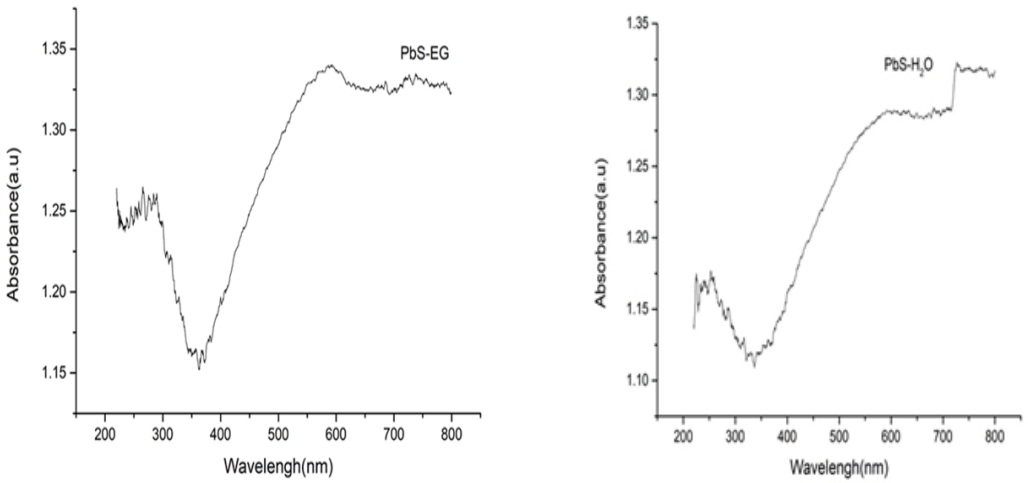

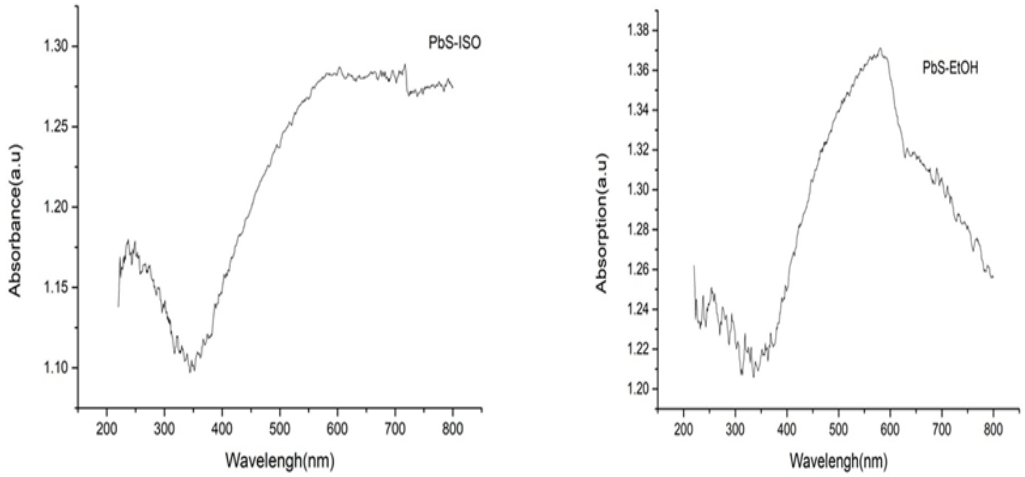

Figure 4. The UV–vis absorbance spectrum of PbS nanoparticles prepared by microwave irradiation method in various solvents. Ethylene glycol (EG), Distilled water (H_2O), Ethylene alcohol (EtOH), and Isopropanol (ISO)**.**

The band gap energy of the PbS–EG nanoparticles is calculated to be 2.53 eV, which is greater than 0.41 eV (bulk PbS). Among the four samples, the PbS synthesized in ethylene glycol (PbS–EG) obtains the smallest particle size with higher band gap energy. Table 2 presents the band gap energy of each sample respectively. The dependence of the energy of electron transitions between the quantized levels of the valance and conduction bands on the particle size is used to estimate the particle size. Such transition is often called excitonic because an electron–hole pair generated by light absorption is similar to the Wannier–Mott exciton in a bulk crystal. The decrease in particle size, as well as the increase in band gap energy of the as–prepared nanoparticles, signify the size quantization effects [30]. Size quantization of the charges in a small volume crystallite is well known for forming the blue shift.

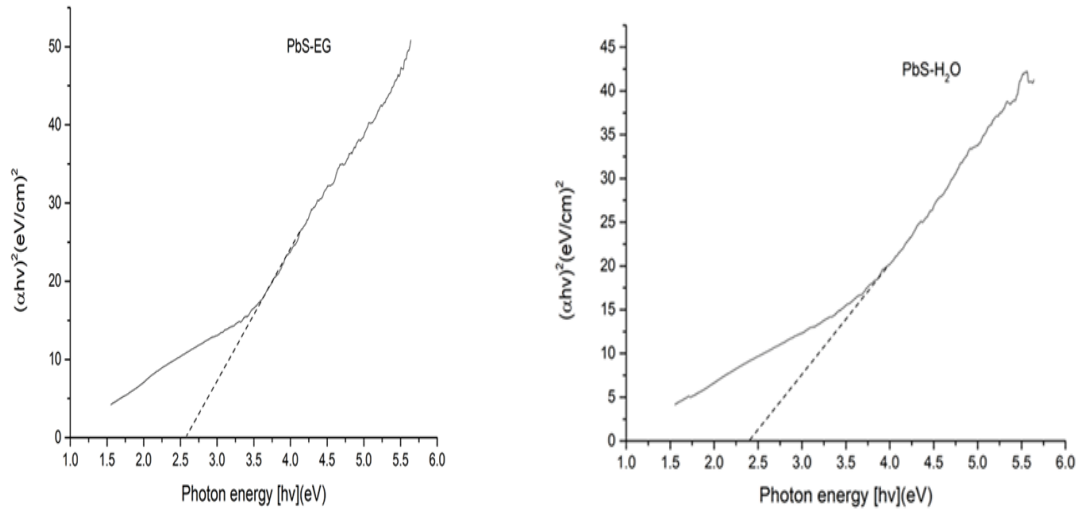

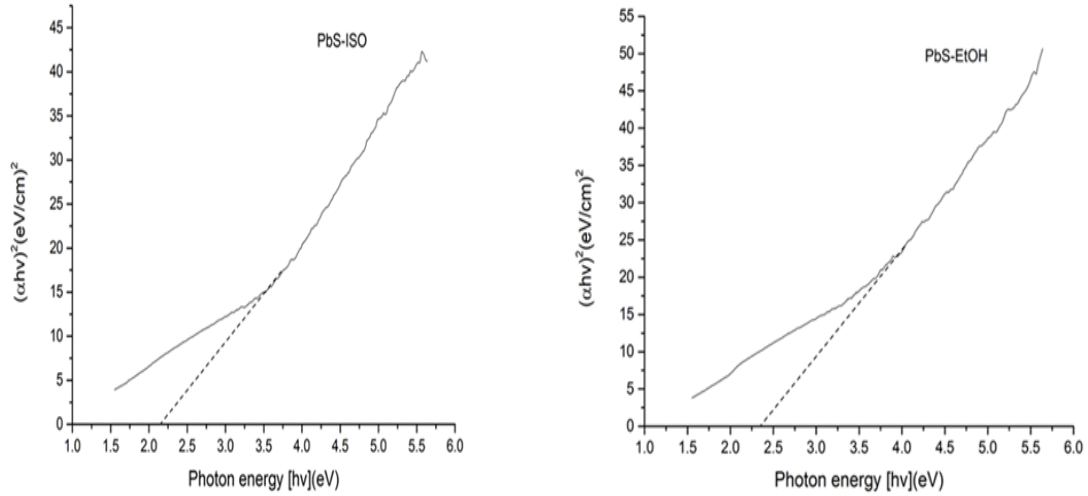

Figure 5. The Plot of $(\alpha h\upsilon)^2$ vs $h\upsilon$ for direct transitions of as prepared PbS nanoparticles in various solvents, where α is absorption coefficient and $h\upsilon$ is photo energy. Band gap energy, E_g is obtained by extrapolation to α = 0.

Table 2. The Band gap energy and the diameter of the particles sizes determined from TEM images

Sample	Bandgap (eV)	ΔE (eV)	Dipole moment (D)	Range of particle sizes (nm)
PbS–EG	2.53	2.12	2.2	28–40
PbS–H_2O	2.41	2.00	1.8	34–44
PbS–EtOH	2.36	1.95	1.7	42–50
PbS–ISO	2.20	1.59	1.6	52–60

Furthermore, the energy of the band gap of the as–prepared samples increases with the increase in dipole moment of the solvent which corresponds with the decrease in particle size.

To explain the role of solvents in the formation of different particle sizes of PbS nanoparticles, several experimental controls were carried out. In dealing with polar solvents with microwave irradiation synthesis, high and uniform heating could be provided, and the temperature gradients can be avoided, providing a uniform environment for the nucleation of nanoparticles [31]. This result confirmed that the behaviour of the polar solvent under the influence of irradiation from microwave has a close relationship with its polarity; the increasing absorption ability of microwave energy resulted from increasing polarity [18]. Besides the temperature and the compositions of the material, the dielectric properties of the solvents play a significant role in the nucleation of the nanoparticles.

The dielectric constant of the material represents its ability to be polarized due to the external electric field [32]. The dielectric constant and the dipole moment are strongly correlated since the

dielectric constant is a function of the dipole moment of the molecule. Moreover, a solvent with a high dielectric constant tends to stabilize the ions [33]. Hence, the microwave absorptive ability could be judged by the criteria of the dipole moment. These results indicated that the PbS nanoparticles with a smaller size of about 34.8 nm were obtained in ethylene glycol as it has the best dispersion condition. Moreover, due to the higher dipole moment of Ethylene glycol solvent, the rapid heating under the microwave irradiation accelerates the nucleation of PbS nanoparticles. However, in isopropanol, PbS nanoparticles did not show such good dispersion, and the particle size of about 56.7 nm was obtained. The low dipole moment of isopropanol solvent plays a role in the formation of the large–sized nanoparticles. Therefore, ethylene glycol with a high permanent dipole is an excellent solvent to be used in a microwave irradiation synthesis.

3.3. Influence of Microwave Irradiation time

Figure 6 shows the XRD spectrum of PbS nanoparticles synthesized with different irradiation time. The results show a cubic crystalline phase of PbS with no other peaks for impurities.

In all the spectrums, nine sharp peaks are located within 2θ range of 25.996, 30.106, 43.097, 51.021, 53.466, 62.587, 68.947, 71.004 and 79.012 were matched perfectly with the (111), (200), (220), (311), (222), (400), (331), (420), and (422) crystalline plane with cubic structure of PbS reported in ICDD PDF 96–901–3404, with 5.93A^{c} as the lattice parameters and 208.7 $A^{\circ 3}$ as the cell volume.

The crystallite sizes of the nanoparticles were obtained using Scherrer's equation, and the estimated particle sizes are listed in Table 3. The results show that the broadening peaks (FWHM) at a shorter irradiation time are larger than at a longer irradiation time. This broadness explains the mean crystallite sizes of the samples.

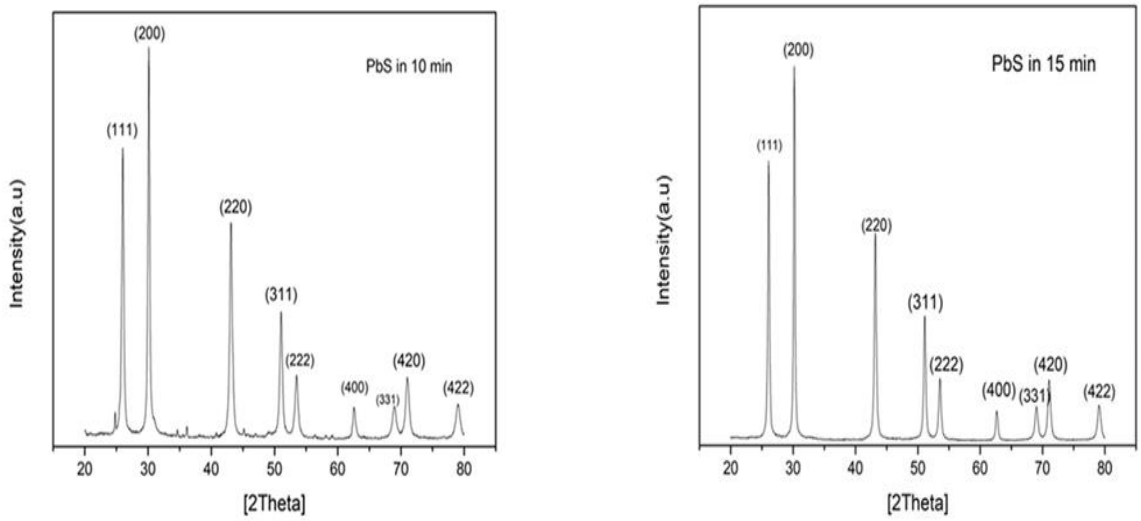

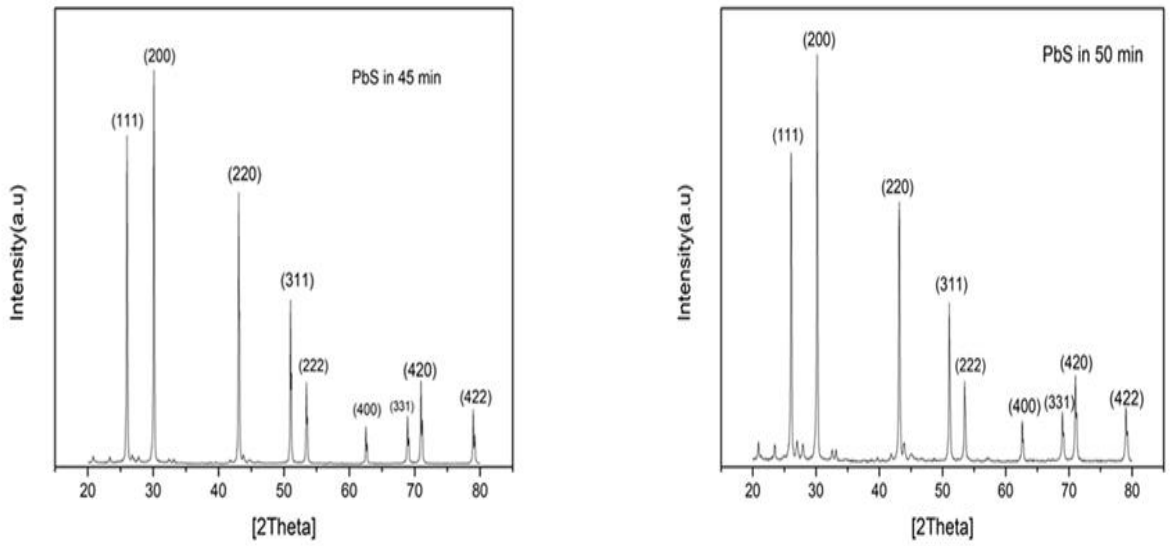

Figure 6. X–ray diffraction patterns of PbS nanoparticles prepared in different irradiation time using ethylene alcohol.

Table 3. XRD results of PbS nanoparticles in different irradiation time

Samples	Irradiation time (min)	FWHM of $(200)(2\theta)$	Intensity of $(200)(2\theta)$	Crystallite size (nm)
PbS–1	10	0.35199	11565.616	39.2
PbS–2	15	0.28584	17821.778	46.5
PbS–3	45	0.18794	12043.605	100.28
PbS–4	50	0.16118	21776.481	100.29

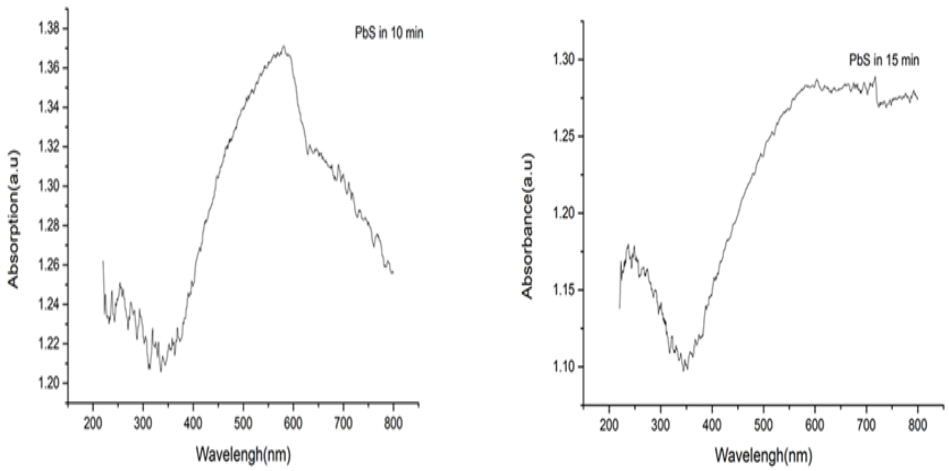

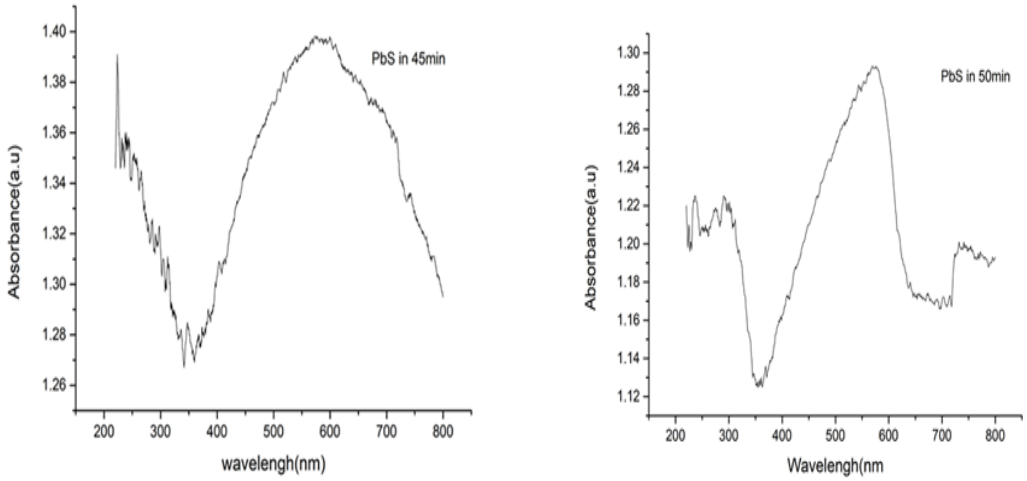

Figure 7. The UV–vis absorbance spectrum of PbS nanoparticles prepared by microwave irradiation method in different irradiation time.

Figure 7 shows the UV–vis absorption spectra of PbS nanoparticles synthesized using the microwave irradiation method in different irradiation time. The products also indicate the two peaks with strong absorptions. Both the two peaks can also be assigned to the exciton transitions from the samples.

The energy band gap (E_g) of PbS nanoparticles can be evaluated from the UV–vis spectra using Tauc plot of $(h\nu\alpha)^2$ versus $(h\nu)$ and the extrapolating from the linear line portion of the curves to the energies axis. Figure 8 shows the Tauc plots of the samples.

The blue shift of the absorption edge in comparison to the bulk PbS clearly explains the quantum conferment effect of the PbS nanoparticles.

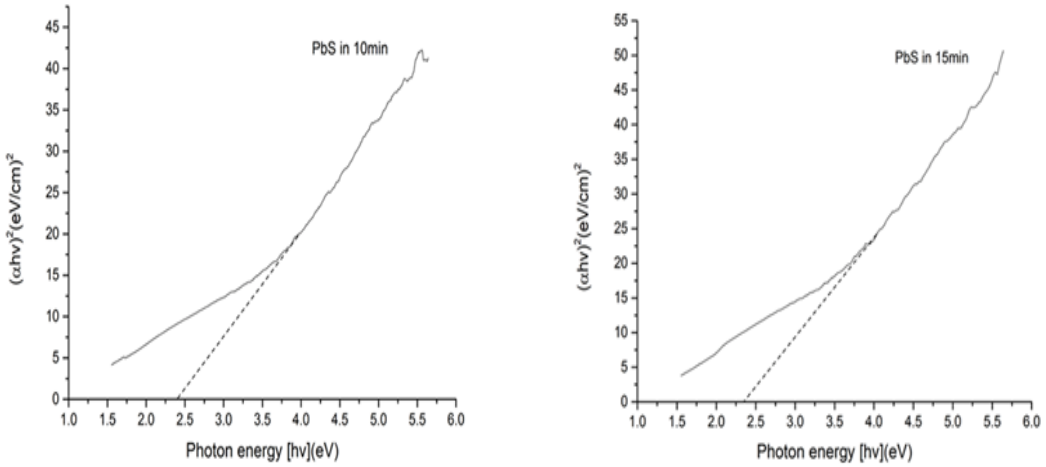

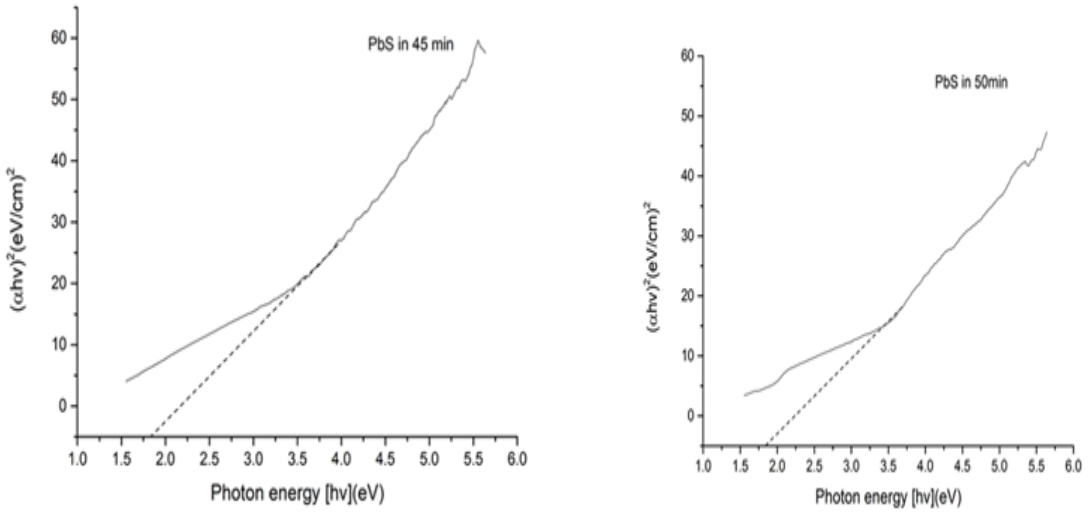

Figure 8. The plot of $(\alpha\ h\upsilon)^2$ vs $h\upsilon$ for direct transitions of as prepared PbS nanoparticles in different irradiation time, where α is absorption coefficient and $h\upsilon$ is the photon energy. Band gap energy, E_g is obtained by extrapolation to α = 0.

Table 4. The Band gap energy and the corresponding blue shift energy (Δ*E*) of the samples

Samples	Irradiation time (min)	Band gap (eV)	ΔE (eV)	Crystallite sizes (nm)
PbS–1	10	2.41	2.0	39.2
PbS–2	15	2.36	1.95	46.5
PbS–3	45	1.61	1.2	100.28
PbS–4	50	1.60	1.19	100.29

The band gap energy of each sample is listed in Table 4, as shown in this table; the estimated band gap reduces with the increase in the irradiation time.

The result from Table 4 shows that the band gap energy decreases with the increase in the irradiation time; this is related to the particle sizes of the samples. The smaller the particle size, the larger the band gap of the samples due to the quantum conferment effect of the samples. This result clearly shows that a longer irradiation time influences Ostwald ripening due to its effect on the interfacial energy, growth rate coefficients, and solubility which can increase the particle size. The microwave quantum energy is much less than the ionization energies of the compounds. This energy

can act as non–ionizing radiation that causes the molecular motions of the ions and the rotation of the dipoles but it does not affect the molecular structure.

3.4 Analytical Applications

As can be seen from the x–ray diffraction patterns of PbS nanoparticles (Fig 2 and Fig 6), different nanoparticles sizes of 34.8, 39.2, 46.5 and 56.7 nm were synthesized. These results confirmed that each particle size will have different electronic structures and separations of energy level. In addition, the ability of nanoparticles to react, depends on particle sizes. Nanocrystals of semiconductor also acquired considerable attentions in the area of both electrochemical and photoelectrochemical biosensors [34, 35]. In photoelectochemical analysis, semiconductor nanomaterials possessed properties for its potential applications in photoelectric biosensors [36]. The pairs of electron–hole were generated in the valence band and the conduction–band with irradiation from the light energy directly to the semiconductor nanomaterials. The excitation of these charge carries within the nanomaterials and substrate could improve redox processes on the electrode [37]. The high surface–to–volume ratio and size–dependent electronic properties of semiconductor nanoparticles also provide an intriguing and useful entity in the research fields. These properties from various nanoparticle sizes and structures can yield different catalytic activities [38, 39]. When a nanoparticles exhibits electrocatalytic activity against the reaction of interest collides with the electrode, it catalyzes the reaction and resulted in a large current increase. The particle sizes of the nanoparticles are exactly related to the increase in current, allowing nanoparticles size representation. In electrocatalytic analysis, nanoparticles are considered as a whole, with abundant nanoparticles disable on an electrode [40]. In this manner, nanoelectrodes facilitate electrochemical analysis to be transported at time scales and in media unfeasible accepting larger electrodes. Another critical outcome of scaling down electrode size is that radial diffusion is the effective form of mass transport to the surface of the nanoelectrode. Therefore, for the application purpose, these nanoparticles sizes may offer a simple and efficient approach to make up different PbS based electrochemical and photoelectrochemical biosensors.

4. CONCLUSION

Lead sulfide (PbS) nanoparticles with different particle sizes have been successfully synthesized using various solvents under microwave irradiation method using $CH_3(COO)_2Pb.3H_2O$ and CH_3CSNH_2 as the starting materials. The experimental results show that the solvent property could affect the crystal structure of the final products. The formation mechanism of the PbS nanoparticles can be proposed. The research also shows that the particle sizes of the products increase as the irradiation time decreases. The microwave irradiation method is confirmed to be simple and efficient as well as environmentally friendly. This access may also apply to other materials.

ACKNOWLEDGEMENTS
The authors are thankful to the Department of Physics, Universiti Putra Malaysia for providing the facilities during the research was conducted and also appreciate the financial support provided by Universiti Putra Malaysia under the grant, GERAN PUTRA BERIMPAK (9597200).

References

1. Y. Shirasaki, G. J. Supran, M. G. Bawendi and V. Bulović, *Nature Photonics,* 7 (2013) 13.
2. A. D. Franklin, *Science,* 349 (2015) 2750.
3. V. Adinolfi, I. J. Kramer, A. J. Labelle, B. R. Sutherland, S. Hoogland and E. H. Sargent, *ACS nano,* 9 (2015) 356.
4. D. Sahoo, A. Mandal, T. Mitra, K. Chakraborty, M. Bardhan and A. K. Dasgupta, *Journal of agricultural and food chemistry,* 66 (2018) 414.
5. E. Katz, I. Willner and J. Wang, *Electroanalysis,* 16 (2004) 19.
6. J. Wang, *Analytica Chimica Acta,* 500 (2003) 247.
7. X. Luo, A. Morrin, A. J. Killard and M. R. Smyth, *Electroanalysis,* 18 (2006) 319.
8. A. M. Nightingale, *Journal of Materials Chemistry C,* 4 (2016) 8454.
9. J. D. Patel, F. Mighri, A. Ajji and S. Elkoun, *Materials Sciences and Applications,* 3 (2012) 125.
10. E. Esakkiraj, K. Mohanraj, G. Sivakumar and J. Henry, *Optik-International Journal for Light and Electron Optics,* 126 (2015) 2133.
11. Y. Mulugeta and H. Woldeghebriel, *International Journal of Quantum Chemistry,* 115 (2015) 197.
12. D. Alima, Y. Estrin, D. H. Rich and I. Bar, *Journal of Applied Physics,* 112 (2012) 1143.
13. P. Kush and S. Deka, *Materials Chemistry and Physics,* 162 (2015) 608.
14. D. Nagao, J. Fukushima, Y. Hayashi and H. Takizawa, *Ceramics International,* 41 (2015) 14021.
15. M. A. Mahjoub, G. Monier, C. Robert-Goumet, F. o. Réveret, M. Echabaane, D. Chaudanson, M. Petit, L. Bideux and B. Gruzza, *The Journal of Physical Chemistry C,* 120 (2016) 11652.
16. D. Wang, F. Wang, Y. Wang, Y. Fan, B. Zhao and D. Zhao, *The Journal of Physical Chemistry C,* 119 (2015) 2798.
17. G. J. Lee, S. Anandan, S. J. Masten and J. J. Wu, *Industrial & Engineering Chemistry Research,* 53 (2014) 8766.
18. Y. Hamanaka, W. Oyaizu, M. Kawase and T. Kuzuya, *Journal of Nanoparticle Research,* 19 (2017) 9.
19. J. Y. Kim, J. Yang, J. H. Yu, W. Baek, C. H. Lee, H. J. Son, T. Hyeon and M. J. Ko, *ACS nano,* 9 (2015) 11286.
20. L. s. Grajciar, *The Journal of Physical Chemistry C,* 120 (2016) 27050.
21. V. V. Poborchii, *Solid state communications,* 107 (1998) 513.
22. N. Finlayson, W. Banyai, C. T. Seaton, G. I. Stegeman, M. O'Neill, T. Cullen and C. Ironside, *JOSA B,* 6 (1989) 675.
23. P. Kunal, H. Li, B. L. Dewing, L. Zhang, K. Jarvis, G. Henkelman and S. M. Humphrey, *ACS Catalysis,* 6 (2016) 4882.
24. X. H. Liao, J. J. Zhu and H. Y. Chen, *Materials Science and Engineering: B,* 85 (2001) 85.
25. J. Yang, Y. Hu, J. Luo, Y.-H. Zhu and J. S. Yu, *Langmuir,* 31 (2015) 3500.
26. T. Ding, J. R. Zhang, S. Long and J.-J. Zhu, *Microelectronic engineering,* 66 (2003) 46.

27. R. Saran and R. J. Curry, *Nature Photonics*, 10 (2016) 81.
28. K. Z. Du, X. H. Qi, M. L. Feng, J. R. Li, X. Z. Wang, C. F. Du, G. D. Zou, M. Wang and X. Y. Huang, *Inorganic chemistry*, 55 (2016) 5110.
29. G. Mondal, P. Bera, A. Santra, S. Jana, T.N. Mandal, A. Mondal, S.I. Seok and P. Bera, *New Journal of Chemistry*, 38 (2014) 4774.
30. Y. Cao, P. Hu and D. Jia, *Nanoscale research letters*, 7 (2012) 668.
31. R. Sathyamoorthy and L. Kungumadevi, *Advanced Powder Technology*, 26 (2015) 355.
32. V. Veeraputhiran, V. Gomathinayagam, A. Udhaya, K. Francy and B. Kathrunnisa, *Journal of Advanced Chemical Sciences*, 1 (2015) 17.
33. G. Alagumuthu and R. Kirubha, *Open Journal of Synthesis Theory and Applications*, 1 (2012) 13.
34. S. Zhou, Y. Kong, Q. Shen, X. Ren, J. R. Zhang and J. J. Zhu, *Analytical chemistry*, 86 (2014) 11680.
35. Z. D. Meng, K. Ullah, L. Zhu, S. Ye and W. C. Oh, *Journal of the Korean Ceramic Society*, 51 (2014) 307.
36. F. Xiao, Y. Lai, N. Zhang, J. Bai, Y. Xian and L. Jin, *Chinese Journal of Chemistry*, 30 (2012) 1168.
37. J. Du, X. Yu, Y. Wu and J. Di, *Materials Science and Engineering: C*, 33 (2013) 2031.
38. R. D. Tilley and J. J. Gooding, *Nature Energy*, 1 (2016) 16174.
39. D. Gao, H. Zhou, J. Wang, S. Miao, F. Yang, G. Wang, J. Wang and X. Bao, *Journal of the American Chemical Society*, 137 (2015) 4288.
40. S. E. Kleijn, S. C. Lai, T. S. Miller, A.I. Yanson, M. T. Koper and P. R. Unwin, *Journal of the American Chemical Society*, 134 (2012) 18558.